Bull. Mater. Sci., Vol. 34, No. 1, February 2011, pp. 89–95. © Indian Academy of Sciences.

Structure refinement of polycrystalline orthorhombic yttrium substituted calcium titanate: $Ca_{1-x}Y_xTiO_{3+\delta}$ ($x = 0{\cdot}1$–$0{\cdot}3$)

RASHMI CHOURASIA and O P SHRIVASTAVA*
Department of Chemistry, Dr H.S. Gour University, Sagar 470 003, India

MS received 23 May 2007; revised 7 September 2010

Abstract. **The perovskite ceramic phases with composition $Ca_{1-x}Y_xTiO_{3+\delta}$ (where $x = 0{\cdot}1$, $0{\cdot}2$ and $0{\cdot}3$; hereafter CYT-10, CYT-20 and CYT-30) have been synthesized by solid state reaction at 1050°C. The structure refinement using general structure analysis system (GSAS) software converges to satisfactory profile indicators such as Rietveld parameters: Rp, R_{wp}, RF^2 and goodness of fit. The title phases crystallize at room temperature in the space group *Pbnm* (#62) with $a = 5{\cdot}3741(4)$ Å, $b = 5{\cdot}4300(4)$ Å, $c = 7{\cdot}6229(5)$ Å and $Z = 4$. Major interatomic distances, bond angles and structure factors have been calculated from the step analysis data of the compound. The crystal morphology has been examined by scanning electron microscopy. Energy dispersive X-ray (EDX) analysis of the specimens show that yttrium enters into the structural framework of $CaTiO_3$. The particle size of the ceramic phases along major reflection planes ranges between 12 and 40 nm. The polyhedral (CaO_8 and TiO_6) distortions and valence calculations from bond strength data are also reported.**

Keywords. **Perovskites; powder X-ray diffraction; Rietveld refinement; GSAS; nanoceramic.**

1. Introduction

Perovskite type oxides of general formula ABO_3 are well known for their property of cationic substitution on A site (Goodenough *et al* 1976; Myhra *et al* 1986; Ringwood 1985; Shrivastava and Shrivastava 2002). Such materials have received attention due to their variety of applications in making electronic devices. They dominate the low and medium permittivity range of microwave dielectrics and temperature stable ceramics providing high quality factor (Janear *et al* 2001; Kim *et al* 2002; Kipkoetch *et al* 2003). Moreover, the versatility of perovskite structure opens up possibility of making solid solutions designed to achieve specific requirements. $CaTiO_3$ has also been identified as a potential material for long-term immobilization of radioactive cations such as trivalent actinides (Cm^{3+}, Am^{3+}, Pu^{3+}) and rare earth (Gd^{3+}, La^{3+}) cations. Immobilization of Sr^{2+}, U^{4+}, Y^{3+} and Ba^{2+} has also been reported in $CaTiO_3$, which is one of the major constituents of 'Synroc' precursor assemblage (Ringwood 1978; Ringwood *et al* 1979; Shrivastava *et al* 2004). In order to understand the mechanism of immobilization of Y^{3+} ion in $CaTiO_3$ through crystallochemical interaction, a simulation study of yttrium substituted calcium titanate of composition $Ca_{1-x}Y_xTiO_{3+\delta}$ ($x = 0{\cdot}1$, $0{\cdot}2$ and $0{\cdot}3$) have been undertaken.

*Author for correspondence (dr_ops11@rediffmail.com)

2. Experimental

2.1 *Ceramic route synthesis of $Ca_{1-x}Y_xTiO_3$ ($x = 0{\cdot}1$–$0{\cdot}3$) phases*

Calculated quantities of AR grade $CaCO_3$, Y_2O_3 and TiO_2 for the stoichiometry $Ca_{1-x}Y_xTiO_3$ (where $x = 0{\cdot}1$, $0{\cdot}2$ and $0{\cdot}3$) were thoroughly mixed with 15 ml glycerol medium in a mortar-pestle. The synthesis of the ceramic powder was carried out by repeated grinding and sintering the glycerol paste at 1050°C in a muffle furnace. After 72 h of sintering, densification of materials took place and polycrystalline solid solutions were formed.

2.2 *Characterization*

The powder X-ray diffraction data was recorded on Rigaku RUH3R diffractometer at a step size of $0{\cdot}02°$ between $2\theta = 5$–$90°$ with a counting rate of 2 s/step. In all 4251 data, points were subjected to GSAS programming. Scanning electron microscopy and EDX analysis were carried out on Jeol JSM-5600 electron microscope at an accelerating voltage of 20 kV.

3. Results and discussion

3.1 *Rietveld refinement and crystallographic model of phases*

All prominent reflections of the X-ray diffraction patterns of the $Ca_{1-x}Y_xTiO_{3+\delta}$ ($x = 0{\cdot}1$, $0{\cdot}2$ and $0{\cdot}3$) have been indexed

for orthorhombic system constrained by operators of space group *Pbnm* (#62). In samples CYT-10, CYT-20 and CYT-30, the intensity and positions of all major reflections match with those of parent perovskite structure of $CaTiO_3$ (Liu and Liebermann 1993) (figure 1). However, in CYT-30 traces of minor secondary phases of CaY_4O_7 ($d = 2{\cdot}94$ Å) and Y_2O_3 ($d = 3{\cdot}06$ Å) have also been observed (peaks marked with *). The Rietveld refinement of crystal data of phase pure CYT-10 was performed by the least square method using GSAS software (Larson and Von Dreele 2000) (figure 2). The reflection conditions for the chosen space group were verified from the international table for X-ray crystallography and checked by presence of $\overline{021}$ and absence of $\overline{201}$ reflections, which are not allowed (Bouchard and Weither 1972; JCPDS file no. 82–0232 1974; Wise *et al* 2001; Mitchell and Liferovich 2004). Other systematically absent reflections in support of chosen space group were also verified by Intensity Statistics (ISTATS) software. In addition to these, both odd-odd-odd and odd-odd-even reflections are present in the title phase indicating that the oxygen octahedra are tilted both in phase as well as antiphase (Glazer 1972).

The normal probability plot for the histogram gives nearly a straight line indicating that the I_0 and I_C values are for the most part normally distributed with a slope of 1·2059 (figure 3). The crystal data was derived from the crystal information file prepared after final cycle of refinement by Rietveld analysis (Rietveld 1969). The accuracy of the fit is indicated by agreement in the expected and calculated R-factors and goodness of fit (table 1). The final refinement was carried out with occupancies constrained at Ca = 90% and Y = 10%, which matches with the composition of the representative sample of the ceramic powder.

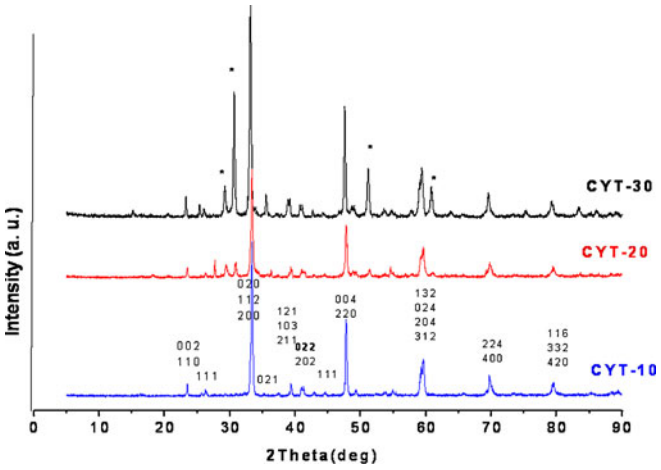

Figure 1. X-ray diffraction patterns of $Ca_{1-x}Y_xTiO_{3+\delta}$ ($x = 0{\cdot}1$, 0·2 and 0·3) ceramic phases along with the indexed reflections.

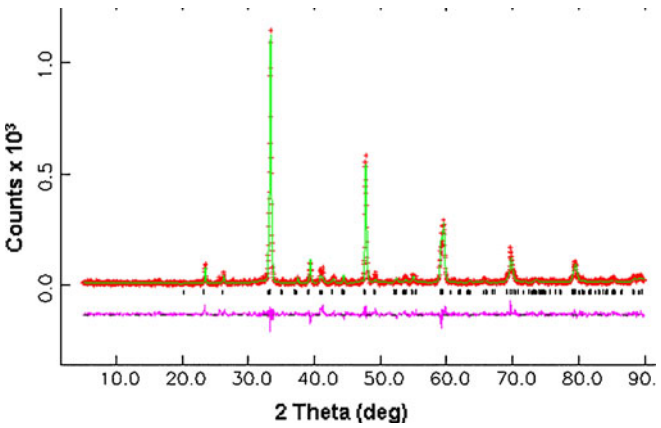

Figure 2. Rietveld refinement plot for $Ca_{0{\cdot}90}Y_{0{\cdot}10}TiO_{3+\delta}$ ceramic sample showing observed (+), calculated (continuous line) and difference (lower) curves. The vertical bars denote Bragg reflections of the crystalline phase.

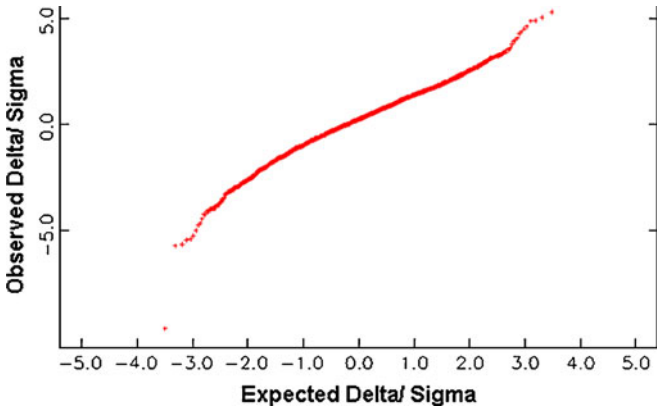

Figure 3. Probability plot between I_0 and I_C for polycrystalline $Ca_{0{\cdot}90}Y_{0{\cdot}10}TiO_{3+\delta}$ ceramic sample.

Table 1. Crystallographic data for polycrystalline $Ca_{0{\cdot}9}Y_{0{\cdot}1}TiO_{3+\delta}$ at room temperature.

Structure	Orthorhombic
Space group	*Pbnm* (#62)
Lattice parameters	$a = 5{\cdot}3741(4)$ Å
	$b = 5{\cdot}4300(4)$ Å
	$c = 7{\cdot}6229(5)$ Å
	$\alpha = \beta = \gamma = 90{\cdot}0$
Z	4
Rwp	0·2421
Rp	0·1735
wR_{expected}	0·1899
RF^2	0·15122
Volume of unit cell	222·449(16) Å^3
Unit cell formula weight	565·523
$\text{Density}_{X\text{-}ray}$	4·222
Goodness of fit (S)	1·28
D_{wd}	1·366
Slope	1·2022

Table 2. Final refined lattice parameters, atomic coordinates and Rietveld parameters of CYT-10 ceramic phase at room temperature.

Atom	*x*	*y*	*z*	Occupancy	U_{iso} (Å^2)
Ti1	0·00	0·50	0·0	1·00	0·01847
Ca2	0·97535	0·02271	0·25	0·9130	0·01159
Y3	0·97535	0·02271	0·25	0·10	0·01159
O4	0·1240	0·430	0·25	1·0	0·01866
O5	0·7106	0·3029	0·03325	1·0	0·01866

Table 3. Selected interatomic distances (Å), O–M–O angles and polyhedral distortions for CYT-10 ceramic powder.

Ca2/Y3–O4	2·35144(16)	Ca2/Y3–Ca2/Y3	4·01067(21)*2
Ca2/Y3–O4	2·21120(15)	Ca2/Y3–Ca2/Y3	3·82860(23)*2
Ca2/Y3–O5	2·65877(11)*2	Ca2/Y3–Ca2/Y3	3·63838(19)*2
Ca2/Y3–O5	2·27007(9)*2	Ti1–O4	2·05435(11)*2
Ca2/Y3–O5	2·67528(12)*2	Ti1–O5	2·01255(11)*2
Ca2/Y3–Ti1	3·42131(19)*2	Ti1–O5	1·90487(10)*2
Ca2/Y3–Ti1	3·21965(17)*2	Ca2/Y3–Ti1	3·18949(16)*2
Ca2/Y3–Ti1	3·40539(18)*2		
Bond angles (*deg.*)			
O4–Ti1–O4	180·0(0)	O4–Ca2–O5	130·6439(18)*2
O4–Ti1–O5	92·1466(25)*2	O4–Ca2–O5	107·9959(28)*2
O4–Ti1–O5	102·5210(20)*2	O4–Ca2–O5	67·6926(26)*2
O4–Ti1–O5	87·8534(25)*2	O5–Ca2–O5	93·412(5)
O4–Ti1–O5	77·4789(20)*2	O5–Ca2–O5	121·172(4)
O5–Ti1–O5	89·041(5)*2	O5–Ca2–O5	67·231(5)*2
O5–Ti1–O5	180·000(0)	O5–Ca2–O5	123·497(4)*2
O5–Ti1–O5	90·959(5)*2	O5–Ca2–O5	63·178(4)*2
O5–Ti1–O5	179·9657(0)	O5–Ca2–O5	121·172(4)*2
O4–Ca2–O4	83·2992(32)	O5–Ca2–O5	76·842(4)
O4–Ca2–O5	69·121(4)*2	O5–Ca2–O5	168·9843(6)*2
O4–Ca2–O5	130·0958(21)*2	O5–Ca2–O5	78·855(4)*2
O4–Ca2–O5	60·4322(17)*2		
Polyhedral distortions (Å)		CaO_8	TiO_6
Δ ($\times 10^4$)		52·80	10·01

$\Delta = 1/n \sum \{(R_i - R_m) / (R_m)\}^2$ where $n = 8$ and 6 for eight and six coordinations, respectively.
*Indicates the multiplicity of bond; figures in parentheses show the esd values.

The atomic coordinates, isotropic thermal parameters, major interatomic distances and angles data along with polyhedral distortions 'Δ' (Kim *et al* 2007; Shrivastava *et al* 2008) are summarized in tables 2 and 3. The inter-planar spacing and their observed and calculated structure factors have also been determined. The interatomic distances between Ti(1) and the apex oxygen atoms of the octahedron have been found to be 2·05434 Å, whereas the two sets of planar oxygen bond distances Ti(1)–O(5) are 1·90487 and 2·01256 Å, respectively (figure 4). For the given coordination number the calculated M–O distances are close to their standard values of metal oxygen distances in corresponding metal oxides (West 2003). The DIAMOND projection of the crystal model represents appropriately the coordination spheres of Ca and Ti atoms (figure 5). The B site of the perovskite maintains six coordinations with the shortest Ti–O(5) bond of 1·90487 Å and the longest one Ti–O(4) of 2·05434 Å. The distortion of TiO_6 reduces the coordination number of Ca/Y atoms

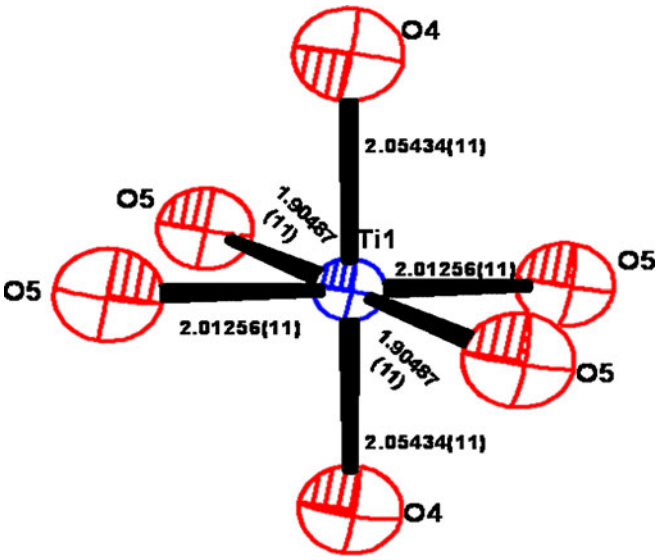

Figure 4. Ortep view of Ti coordination in TiO_6 with their respective bond lengths.

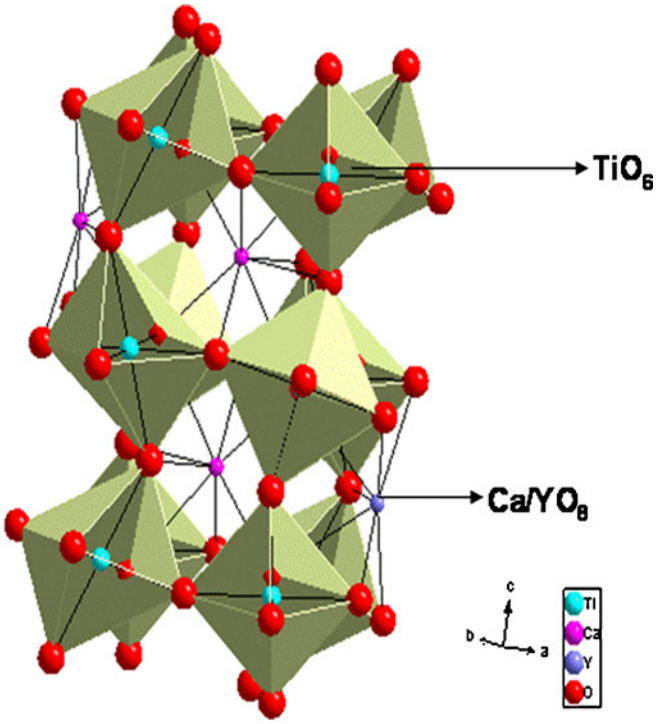

Figure 5. DIAMOND projection of stick and ball representation of coordination sites of Ti and Ca/Y.

to 8, resulting in eight acentric bonds in contrast to twelve for ideal cubic perovskite. The geometry of Ca/Y coordination sphere defined by the tilted octahedra is, therefore, a distorted cuboctahedron in relation to ideal A site polyhedron in cubic perovskite, which has four triangular, and six square faces (Thomas 1996). The bond valence ($V_i = \Sigma b_{ij}$, where $b_{ij} = (R_o/R)^N$) (Shrivastava and Chourasia 2008) for Ca was found to be significantly high confirming residual compression of Ca–O bonds. The compression of the Ca cation is primarily attributed to the partial occupancy by the marginally smaller cation (Y^{3+}) in the perovskite framework. In addition, the displacement of the Ca cation due to octahedral tilting also contributes to the compression of the A-site species. The oxidation state for Ti^{4+} has been found to be 4·08, which is consistent with the expected formal oxidation state of titanium in B site of perovskite structure. The rare-earths and trivalent actinides preferentially replace Ca^{2+}, where charge balance is achieved by partial replacement or substitution of Ti^{4+} by Ti^{3+} (Szajman *et al* 1987; Leturcq *et al* 2001). However, the mechanism of substitution of Ca^{2+} by Y^{3+} in perovskite solid solution needs explanation in terms of charge balance. One of the plausible mechanisms could be the charge compensation through change in perovskite substoichiometry, i.e. by increase of oxygen content.

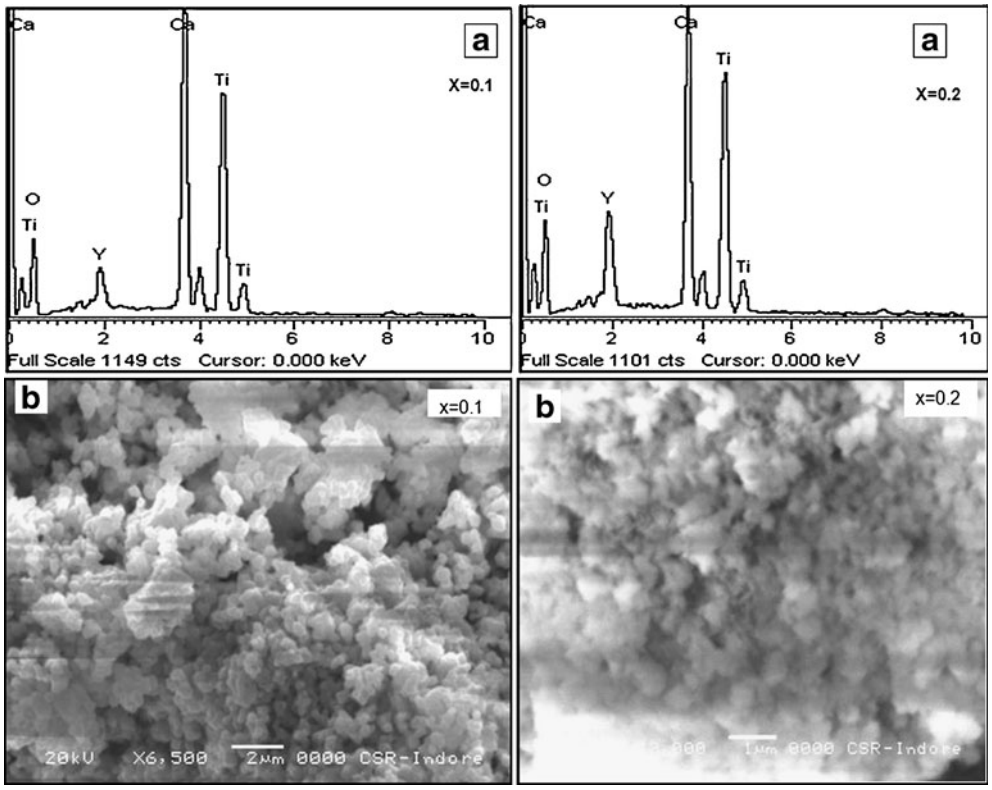

Figure 6. **a**. EDAX spectra and **b**. SEM images of polycrystalline $Ca_{1-x}Y_xTiO_{3+\delta}$ ($x = 0{\cdot}1$ and $0{\cdot}2$) ceramic powders.

Table 4. Distribution of particle size along prominent reflections of $Ca_{1-x}Y_xTiO_{3+\delta}$ ($x = 0{\cdot}1$–$0{\cdot}3$) ceramic phases.

	CYT-10		CYT-20		CYT-30	
h, k, l planes	FWHM (2θ)	Particle size (nm)	FWHM (2θ)	Particle size (nm)	FWHM (2θ)	Particle size (nm)
002	0·20	40·60	0·24	33·83	0·22	36·90
111	0·20	40·82	0·36	22·68	0·28	29·15
200	0·22	37·73	0·28	29·64	0·24	34·56
211	0·26	32·48	0·30	28·15	0·58	14·55
004	0·26	33·45	0·32	27·17	0·28	31·03
312	0·70	13·10	0·60	15·27	0·72	12·71
224	0·42	23·07	0·44	22·02	0·44	22·00
420	0·64	16·17	0·58	17·84	0·70	14·75

Table 5. Selected observed and calculated structure factors of $Ca_{0{\cdot}90}Y_{0{\cdot}10}TiO_{3+\delta}$ ceramic powder. The seven columns within each group contain the values h, k, l, d spacing, F_{osq}, F_{csq} and intensity, respectively. The reflections detected from the final cycles in the least-squares refinement.

h	k	l	d-space	F_{osq}	F_{csq}	Intensity (%)
0	0	2	3·81114	8·439E + 03	5·080E + 03	4·529
0	0	2	3·81144	7·685E + 03	5·080E + 03	2·0588
1	1	1	3·41495	2·382E + 03	1·461E + 03	4·0974
0	2	0	2·71501	6·743E + 04	6·700E + 04	18·2366
0	2	0	2·71501	6·636E + 04	6·700E + 04	8·9584
1	1	2	2·69800	9·363E + 04	9·575E + 04	100·00
1	1	2	2·69800	9·408E + 04	9·575E + 04	50·1581
2	0	0	2·68705	4·815E + 04	4·635E + 04	12·7517
2	0	0	2·68705	4·881E + 04	4·635E + 04	6·4521
1	0	3	2·29713	6·510E + 03	5·992E + 03	2·5114
2	1	1	2·29643	7·549E + 03	8·122E + 03	5·8207
0	2	2	2·21134	1·846E + 04	9·578E + 03	6·5964
1	1	3	2·11561	3·817E + 03	2·849E + 03	2·4948
1	2	2	2·04498	4·951E + 03	6·033E + 03	3·0221
0	0	4	1·90572	2·364E + 05	2·226E + 05	31·3217
2	2	0	1·90984	1·013E + 05	9·161E + 04	26·9611
0	0	4	1·90572	2·343E + 05	2·226E + 05	15·4993
2	2	0	1·90984	9·926E + 04	9·161E + 04	13·1885
1	3	1	1·67348	7·980E + 03	5·449E + 03	3·2728
1	3	2	1·56422	4·646E + 04	5·280E + 04	16·7277
1	3	2	1·56422	4·691E + 04	5·280E + 04	8·4328
0	2	4	1·55982	5·896E + 04	6·353E + 04	10·5580
0	2	4	1·55982	6·006E + 04	6·353E + 04	5·3688
2	0	4	1·55446	5·229E + 04	5·080E + 04	9·3026
3	1	2	1·55347	6·576E + 04	6·258E + 04	23·3691
2	0	4	1·5546	5·383E + 04	5·080E + 04	4·7810
3	1	2	1·55347	6·902E + 04	6·258E + 04	12·2444
0	4	0	1·35750	4·646E + 04	3·574E + 04	3·2258
2	2	4	1·3490	6·807E + 04	5·766E + 04	18·7002
2	2	4	1·3490	6·792E + 04	5·766E + 04	9·3157
4	0	0	1·34353	4·587E + 04	3·267E + 04	3·1280
2	4	0	1·21166	2·548E + 04	2·287E + 04	2·9436
1	1	6	1·20554	4·283E + 04	4·508E + 04	9·8255
3	3	2	1·20763	2·150E + 04	2·180E + 04	4·9448
1	1	6	1·20554	4·297E + 04	4·508E + 04	4·9223
3	3	2	1·20763	2·139E + 04	2·180E + 04	2·4562
0	4	4	1·10567	3·681E + 04	2·640E + 04	3·7779
4	0	4	1·09808	2·994E + 04	2·337E + 04	2·9461

Intensities less than 1% have been omitted.

Within the permissible statistical limits, the EDX analysis shows consistency in observed and theoretical atomic and weight ratios with respect to Y and Ti.

Phase	Y/Ti weight ratio	Y/Ti atomic ratio
CYT-10	0·16 (*calc* 0·18)	0·09 (*calc* 0·10)
CYT-20	0·39 (*calc* 0·37)	0·21 (*calc* 0·20)

The EDX spectra show the presence of yttrium in the polycrystalline phases (figure 6a). The scanning electron micrographs show the typical morphology of the grains, which are about 0·2–0·3 μm in length (figure 6b). The particle size calculation has been done for most of the low angle and high-intensity reflections using Scherrer's formula (Begg *et al* 1998) (table 4). The size distribution along the reflection planes ranges from 12–40 nm for $Ca_{1-x}Y_xTiO_{3+\delta}$ ($x = 0{\cdot}1 - 0{\cdot}3$) ceramic phases. The interplanar spacing and their observed and calculated structure factors are reported in table 5.

The electron density map (Fourier map) of CYT-10 constructed in order to locate atoms (viz. Ca/Y, Ti and O) reflects the form of sliced sections through the structure at regular intervals wherein the peak height is proportional to the number of electrons possessed by a particular atom (figure 7). The relative peak heights with respect to Ca and Ti at different locations have been found to be $1{\cdot}0 \pm 0{\cdot}05$ against the expected value of 1·0. The Fourier plot that shows contour maps of calcium and titanium has three minimum values of charge density between Ti and O atoms due to the presence of three different Ti–O distances in the crystal (0·264, 0·128, and 0·085 electrons per a.u.^{3}). The Ti–O bond is covalent with some partial ionic character. This is due to hybridization effect between Ti–3*d* and O–2*p* states (Shrivastava and Avasthi 1986).

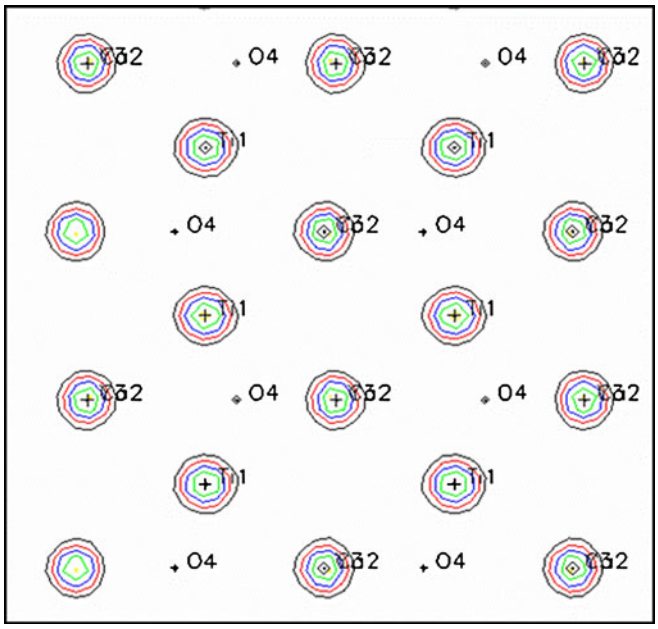

Figure 7. Calculated Fourier map showing contours of charge density of $Ca_{0{\cdot}90}Y_{0{\cdot}10}TiO_{3+\delta}$ ceramic powder.

4. Conclusions

The ceramic phase $Ca_{0{\cdot}9}Y_{0{\cdot}1}TiO_{3+\delta}$ crystallizes in orthorhombic symmetry. The perovskite matrix of calcium titanate can be modified by partial substitution of calcium by yttrium to yield a single phase polycrystalline solid solution. The title ceramic material has perovskite chains of distorted TiO_6 polyhedrons interlinked through Ca/Y atoms. The particle size along prominent reflection planes lies in the range of 12–40 nm. The crystallographic data and the structure model of the title ceramic phase close to composition $Ca_{0{\cdot}9}Y_{0{\cdot}1}TiO_{3+\delta}$ could be useful in the study of structure–property relationship of yttrium-loaded nuclear waste forms.

Acknowledgements

The authors thank the Department of Science and Technology, Government of India, New Delhi, for funding the research project No. SR/S3/ME/20/2005-SERC-Engg under SERC program. Thanks are also due to the Council of Scientific and Industrial Research (CSIR), New Delhi, for awarding a Senior Research Fellowship (Ext.) to one of the authors (RC).

References

Begg B D, Vance E R and Conradson S D 1998 *J. Alloy Compd.* **273** 226

Bouchard R J and Weither J F 1972 *J. Solid State Chem.* **4** 80

Glazer A M 1972 *Acta Crystallogr.* **B28** 3392

Goodenough J B, Hong H Y P and Kalfalas J A 1976 *J. Mater. Res. Bull.* **11** 203

Janear B, Suvorov D and Valant M 2001 *J. Mat. Sci. Leu.* **20** 71

JCPDS file no. 82–0232 1974 *International tables for X-ray crystallography* (Birmingham: Kynoch Press)

Kim M H, Woo C S, Nahm S, Choi C H, Lee H J and Park H 2002 *Mater. Res. Bull.* **37** 605

Kim E S, Chun B S and Kang D H 2007 *J. Eur. Ceram. Soc.* **27** 3005

Kipkoetch E R, Azough F, Freer R, Leach C, Thompson S P and Tang C C 2003 *J. Eur. Ceram. Soc.* **23** 2677

Larson A C and Von Dreele R B 2000 *LANSCE, MS–H805*, Los Alamos National Laboratory LAUR 86–748

Leturcq G, Advocat T, Hart K P, Berger G, Lacombe J and Bonnetier A 2001 *Am. Mineral.* **86** 871

Liu X and Liebermann R C 1993 *Phys. Chem. Miner.* **20** 171

Mitchell R H and Liferovich R P 2004 *J. Solid State Chem.* **177** 4420

Myhra S, Giorgi R, Delogu P and Riviere J C 1986 *J. Mater. Sci.* **23** 1514

Rietveld H M 1969 *Acta Crystallogr.* **2** 65

Ringwood A E 1978 *Safe disposal of high-level nuclear reactor waste: a new strategy* (Canberra: Australian National University Press) p. 64

Ringwood A E, Kesson S E, Ware N G, Hibberson W and Major A 1979 *Nature* **278** 223

Ringwood A E 1985 *Min. Mag.* **49** 159

Shrivastava O P and Shrivastava R 2002 *J. Cryst. Growth Mater. Charact.* **45** 103

Shrivastava O P, Kumar N and Sharma I B 2004 *Bull. Mater. Sci.* **27** 121

Shrivastava S K and Avasthi B N 1986 *J. Less Common Metals* **124** 85

Shrivastava O P and Chourasia R 2008 *J. Chem. Crystallogr.* **38** 362

Shrivastava O P, Chourasia R and Kumar N 2008 *Annals Nucl. Ener.* **35** 1147

Szajman J, Smart R St C and Myhra S 1987 *Surf. Coat. Technol.* **30** 333

Thomas N W 1996 *Acta Crystallogr.* **B52** 31

West A R 2003 *Solid state chemistry and its application* (Singapore: Wiley) p. 710

Wise P L, Reaney I M, Lee W E, Price T J, Iddles D M and Cannell D S 2001 *J. Eur. Ceram. Soc.* **21** 1723